Hindawi Publishing Corporation
International Journal of Rotating Machinery
Volume 2007, Article ID 34901, 10 pages
doi:10.1155/2007/34901

Research Article

Influence of Impeller Geometry on the Unsteady Flow in a Centrifugal Fan: Numerical and Experimental Analyses

M. Younsi, F. Bakir, S. Kouidri, and R. Rey

Laboratoire d'Energétique et de Mécanique des Fluides Interne, Ecole Nationale Supérieure d'Arts et Métiers, 151 boulevard de l'Hôpital, 75013 Paris, France

Received 14 May 2007; Accepted 26 November 2007

Recommended by Ion Paraschivoiu

The aim of this study is to evaluate the influence of design parameters on the unsteady flow in a forward-curved centrifugal fan and their impact on the aeroacoustic behavior. To do so, numerical and experimental studies have been carried out on four centrifugal impellers designed with various geometrical parameters. The same volute casing has been used to study these impellers. The effects on the unsteady flow behavior related to irregular blade spacing, blade count and radial distance between the impeller periphery and the volute tongue have been studied. The numerical simulations of the unsteady flow have been carried out using computational fluid dynamics (CFD) tools based on the unsteady Reynolds averaged Navier Stokes (URANS) approach. The study is focused on the unsteadiness induced by the aerodynamic interaction between the volute and the rotating impeller blades. In order to predict the acoustic pressure at far field, the unsteady flow variables provided by the CFD calculations have been used as inputs in the Ffowcs Williams-Hawkings equations (FW-H). The experimental part of this work concerns measurement of aerodynamic performance of the fans using a test bench built according to ISO 5801 (1997) standard. In addition to this, pressure microphones have been flush mounted on the volute tongue surface in order to measure the wall pressure fluctuations. The sound pressure level (SPL) measurements have been carried out in an anechoic room in order to remove undesired noise reflections. Finally, the numerical results have been compared with the experimental measurements and a correlation between the wall pressure fluctuations and the far field noise signals has been found.

1. INTRODUCTION

Forward-curved centrifugal fans are widely used in industry for their large mass flow rate and their compactness as compared to axial fans. In addition to this, they have a higher total pressure rise as compared to backward fans. Despite their low efficiency, they are employed as circulating fans in central heating and air-conditioning systems in buildings, as blowers in automotive heating-cooling units, and in numerous other applications.

The recent development of CFD techniques for three-dimensional viscous flow fields provides an efficient tool for analysis and design. Thus, flow analysis techniques using the URANS approach have made remarkable progress in turbomachinery applications.

Recently, more attention has been paid to the study of design parameters' effects on the performance and the noise of centrifugal fans. Boltezar et al. [2] studied the influence of irregular blade spacing of car alternator radial fans on the total SPL and the noise spectrum. In their study, they computed the SPL and the spectra values theoretically and compared the values to measured results for several types of fans with different blade spacing. They found that alterations in blade spacing do not significantly alter the total SPL. However, significant dispersion of the sound power over several harmonics was found with irregular fan blade spacing, thus allowing a reduction of the siren effect. They predicted this phenomenon theoretically and confirmed it experimentally. Jeon [3] used the discrete vortex method (DVM) to describe the flow field in a centrifugal fan. He employed the Lowson [4] equation in order to obtain acoustic far field information from the unsteady force fluctuations on the blade. The purpose of his study was to investigate the effects of rotating velocity, flow rate, cutoff distance, and number of blades on the noise. Cho and Moon [5] used the unsteady viscous flow field of a cross-flow fan computed by solving the two-dimensional (2D) incompressible Navier-Stokes equations. They employed the FW-H equation in order to predict the acoustic pressures and to study the acoustic benefit of an impeller with uneven blade

Table 1: Geometrical characteristics of the reference fan.

Reference impeller VA160	
Description	Value
Blade count	39
Impeller width	70 mm
Blade chord length	26.2 mm
Blade thickness	1 mm
Inlet blade angle	5°
Outlet blade angle	70°
Shape blade	circular arc
Impeller inlet diameter	120 mm
Impeller outlet diameter	160 mm
Rotational speed	3000 rpm
Volute casing	
Inlet diameter	120 mm
Outlet size	100 × 76 mm
Volute tongue radius	5 mm
Volute tongue position	Radius 90 mm
Volute shape	Logarithmic law

spacing. Ballesteros-Tajadura et al. [6] performed a three-dimensional numerical simulation of the complete unsteady flow in the whole impeller-volute configuration of an industrial centrifugal fan. They obtained the pressure fluctuations in some locations over the volute wall, and they found a good agreement between the numerical and the experimental results.

In this study, both numerical and experimental approaches are used to evaluate the influence of design parameters on the unsteady flow in a centrifugal fan and their impact on the aeroacoustic behavior.

2. FANS PRESENTATION

In this study, four impellers (VA160, VA160D, VA150, VA160E) designed with various geometrical parameters have been investigated in the same volute casing. The VA160 impeller with 39 blades is considered as the reference. Compared to the VA160, the VA160D presents irregular blade spacing, the VA150 has a different impeller outlet diameter (150 mm), and the VA160E has only 19 blades. The main geometrical characteristics of the reference impeller and the volute casing are presented in Table 1.

Concerning the VA160D impeller, the blade spacing distribution has been obtained using the following equation proposed by the present paper authors:

$$\Delta\theta_b = \frac{360}{z} + k\left[\left(\frac{z}{2\pi\cdot n}\right)\left\{\cos\left[\left(\frac{n\times 2\pi}{z}\right)\left(b-\frac{1}{2}\right)\right]\right\}\left(\frac{\pi}{180}\right)\right], \quad (1)$$

where $k = 50$, $z = 39$, $n = 3$.

This equation gives the blade spacing angle as a sinusoidal function of the blade count b (see, Figure 1). The VA160 fan has a constant blade spacing angle of 9.23 degrees.

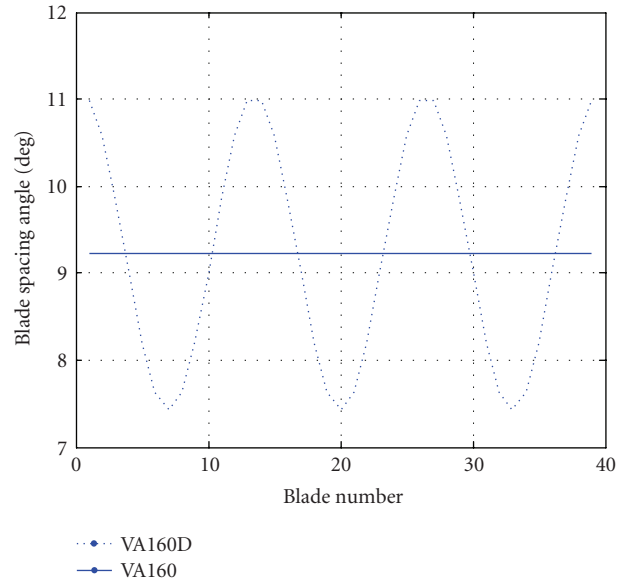

Figure 1: Blade spacing angle distributions.

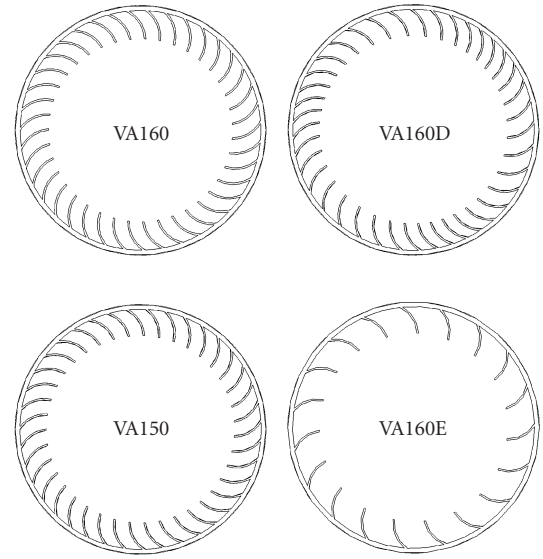

Figure 2: Geometry of the investigated fans.

Figure 2 depicts the geometry for the four impellers under consideration. These parameters have been transformed into a complete 3D computer-aided design model (CAD) in order to build the prototypes for the experimental investigations.

3. EXPERIMENTAL WORK

Overall measurements have been carried out on the test bench shown in Figure 3 designed and built at LEMFI-ENSAM according to the ISO 5801 standard. In order to make these measurements possible, this normalized ducted installation is placed upstream the centrifugal fan making it

(a)

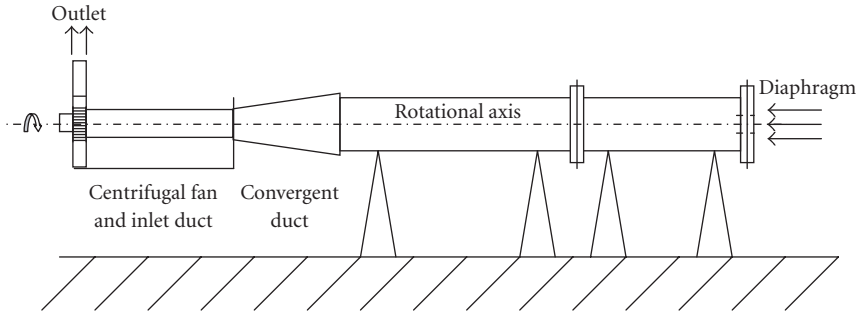

(b)

Figure 3: Test bench and pressure fluctuations measurements at the volute tongue (a) with sketch of the experimental installation (b).

possible to vary the flow rate by changing the diameter of an orificial plate (diaphragm). The rotational speed is set by a frequency converter and measured using an optical tachometer of 0.1% accuracy. For each diaphragm of a given diameter, the static pressure provided by the centrifugal fan is measured using a micromanometer (precision 1%). The experimental work also consists of the measurements of wall pressure fluctuations in the volute casing. Thus, one AREVA 01 dB-Metravib 40 BH 1/4 in. pressure microphone which presents ±0.2 dB uncertainty has been flush mounted on the volute tongue surface. Additionally, one AREVA 01 dB-Metravib 40 AE 1/2 in. free field microphone with ±0.2 dB uncertainty, protected with a nose cone, has been used in order to measure the acoustic pressures. These acoustic measurements have been performed in anechoic room (5.9 × 4.4 × 4.25 m). Background sound pressure level is 18 dB and cut-off frequency is 75 Hz. In order to make these measurements possible, the fan has been adapted on a small airtight box (0.6 m × 0.6 m × 0.6 m), and the conformity to the ISO 5801 standard has been checked. One free field microphone has been positioned one meter away from the fan rotational axis in the same direction of the exit duct (see Figure 4). After the calibration operations, the signals from the microphones have been fed into a personal computer based data acquisition system, and postprocessed using narrow band width analysis.

In order to compare the unsteady flow behavior of the investigated fans at the same operation point (500 m^3/h, 680 Pa), the fans rotational speed has been determined experimentally. Thus, the rotational speeds of the VA160, VA160D, VA150, and VA160E are set to 3000 rpm, 3000 rpm, 3200 rpm, and 2900 rpm, respectively.

4. NUMERICAL MODELING

To consider the unsteady interactions between the rotating impeller blades and the stationary fan casing and to understand the internal flow, a numerical simulation based on the finite volume numerical method using FLUENT 6.2 code has been carried out. The geometrical parameters given in Table 1 have been used in order to generate the computational domain which has been divided into two zones: a rotational zone including the impeller and stationary zone elsewhere. This configuration takes into account the clearance between the impeller and the volute. The inlet and the outlet surfaces of the fan have been extended in order to ensure numerical stability and to minimize boundary conditions effects. The obtained computational domains are shown in Figure 5.

The resulting geometry has been used to build a hybrid mesh. The grid refinement has been studied and adapted to the flow morphology minimizing element distortion and to achieve required resolution in high-gradient regions. The details of this study are reported in previous papers by Younsi et al. [7, 8]. An example of the retained grid mesh

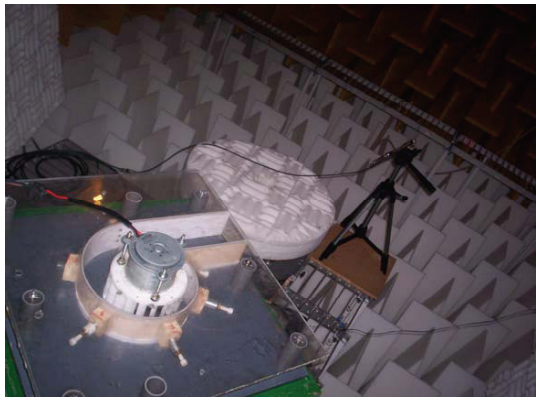

(a)

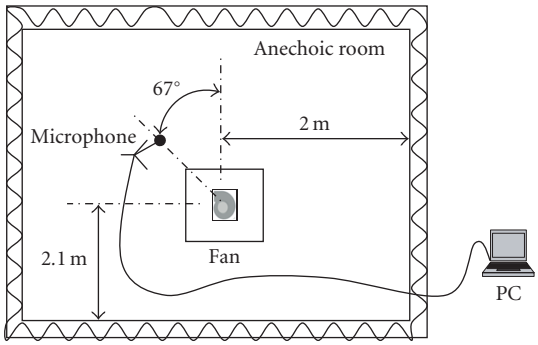

(b)

Figure 4: Acoustic measurements in anechoic room (a) with sketch of the experimental installation (b).

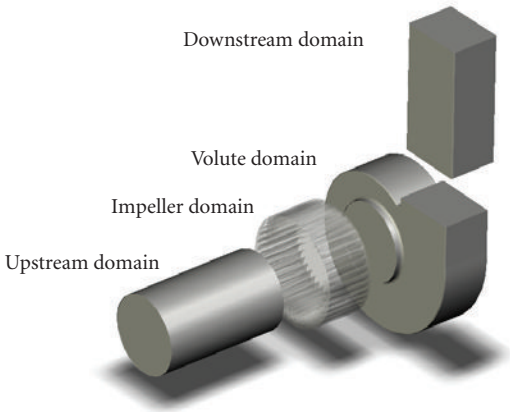

Figure 5: Geometry modeling of the flow domains.

is shown in Figure 6. The meshes generated for all the four fans contain approximately two million elements.

Concerning the numerical simulation parameters, velocity inlet and pressure outlet boundary conditions have been applied at the inlet and the outlet, respectively. According to Majidi [9], a fixed mass flow rate at the inlet of the computational domain is physically unsuitable for unsteady calculations and in particular for considering the rotor/stator interaction. The sliding mesh technique has been applied to the interfaces in order to allow the unsteady interactions between the impeller and the volute casings. Turbulence has been modeled with the k-ω-SST model [10]. The SST model performance has been studied and validated in a large number of cases [11]. It has been shown to perform very well for adverse pressure gradient aerodynamic flows. The maximum residue is lower than or equal to 10^{-4}. The governing equations have been solved using the segregated solver, and a centered simple algorithm has been used for the pressure velocity coupling. The time-dependent term scheme is second order. A gauge pressure of 101325 Pa has been applied to the outlet, and a suitable value has been determined for the inlet. The CFD simulation process began with a steady flow calculation using the frozen-rotor approach. In this case, the relative position of the impeller and casing does not change during the calculations. For unsteady calculations, the grids change their relative position during the calculations according to the angular velocity of the impeller. The time step of the unsteady calculations has been set to 5.10^{-5} seconds. The chosen time step is related to the rotational speed of the impeller as it is small enough to get the necessary time resolution and to capture the phenomena due to the blades passage and their interactions with the volute casing wall. It corresponds to 1/400 of blade passing period. This time step has been approached by the following formulation:

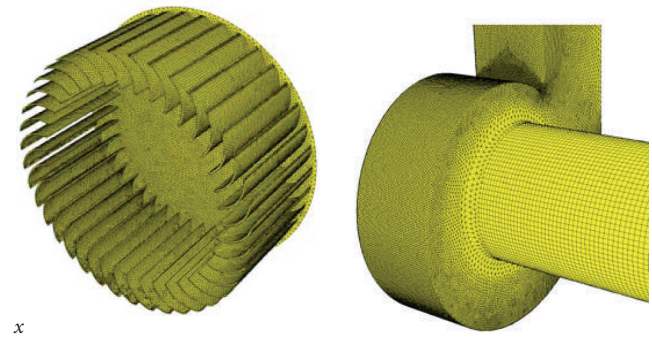

(a) (b)

Figure 6: Retained grid mesh for the VA160 fan.

$$\Delta t \cong \frac{30 \cdot \Delta S}{\pi \cdot N R_2}, \tag{2}$$

where ΔS is set to 2 mm.

The unsteady calculations are carried out for seven impeller revolutions, and the obtained temporal data have been saved for each time step. After windowing the temporal signals using Hamming's window function, each recorded sample has been fast Fourier transform (FFT) processed ($P_{\text{ref}} = 2 \times 10^{-5}$ Pa), and then the aerodynamic pressure spectra have been finally obtained.

5. AEROACOUSTIC CALCULATIONS

The (FW-H) equation [12, 13] is essentially an inhomogeneous wave equation that can be derived by manipulating the

continuity equation and the Navier-Stokes equations. The FW-H equation can be written as follows:

$$\frac{1}{a_0^2}\frac{\partial^2 p'}{\partial t^2} - \nabla^2 p' = \frac{\partial[[\rho_0 v_n + \rho(u_n - v_n)]\delta(f)]}{\partial t} - \frac{\partial[[P_{ij}n_j + \rho u_i(u_n - v_n)]\delta(f)]}{\partial x_i} + \frac{\partial^2}{\partial x_i \partial x_j}[T_{ij}H(f)], \tag{3}$$

where

$$T_{ij} = \rho u_i u_j + P_{ij} - a_0^2(\rho - \rho_0)\delta_{ij},$$
$$P_{ij} = p\delta_{ij} - \mu\left[\frac{\partial u_i}{\partial x_j} + \frac{\partial u_j}{\partial x_i} + \frac{2\partial u_k}{3\partial x_k}\delta_{ij}\right]. \tag{4}$$

The first two source terms in (3) are monopole (thickness) and dipole (loading) sources, respectively, based on their mathematical structure. The monopole source term models the noise generated by the displacement of fluid as the body passes. The dipole or loading source term models the noise that results from the unsteady motion of the force distribution on the body surface. Both of these sources are surface sources, that is, they act only on the surface $f = 0$ as indicated by the Dirac delta function $\delta(f)$. The third source term is a quadrupole source term that acts throughout the volume that is exterior to the data surface as indicated by the Heaviside function $H(f)$.

Using the free-space Green's function ($\delta(G)/4\pi r$ with $G = \tau - t + r/a_0$), the solution of (3) is obtained. Thus, the complete solution consists of surface integrals and volume integrals. The surface integrals represent the contribution from monopole and dipole acoustic sources and partially from quadrupole sources if the integration surface is impermeable. The contribution of the volume integrals which represent quadrupole (volume) sources in the region outside the source surface becomes small when the flow is subsonic. Thus, the volume integrals are neglected. Finally,

$$p'(\vec{x}, t) = p'_T(\vec{x}, t) + p'_T(\vec{x}, t). \tag{5}$$

The two terms on the right of (5), $p'_T(\vec{x}, t)$ and $p'_T(\vec{x}, t)$, thickness and loading terms, respectively, are given by

$$4\pi p'_T(\vec{x}, t) = \int_{f=0}\left[\frac{\rho_0(\dot{U}_n + U_{\dot{n}})}{r(1 - M_r)^2}\right]dS + \int_{f=0}\left[\frac{\rho_0 U_n\{r\dot{M}_r + a_0(M_r - M^2)\}}{r^2(1 - M_r)^3}\right]dS,$$
$$4\pi p'_T(\vec{x}, t) = \frac{1}{a_0}\int_{f=0}\left[\frac{\dot{L}_r}{r(1 - M_r)^2}\right]dS + \int_{f=0}\left[\frac{L_r - L_M}{r^2(1 - M_r)^2}\right]dS + \frac{1}{a_0}\int_{f=0}\left[\frac{L_r\{r\dot{M}_r + a_0(M_r - M^2)\}}{r^2(1 - M_r)^3}\right]dS, \tag{6}$$

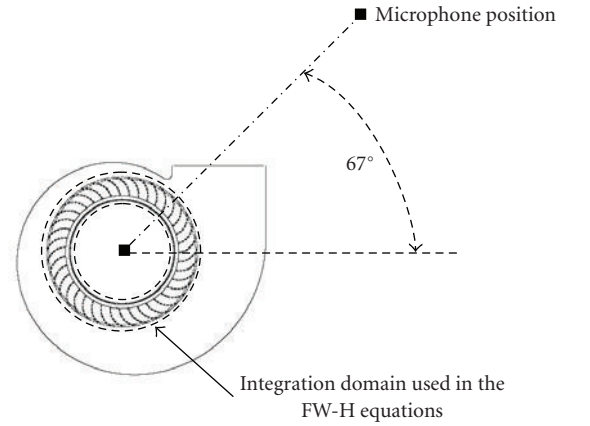

Figure 7: Position of the acoustic pressure calculations and integration domain.

where

$$U_i = v_i + \frac{\rho}{\rho_0}(u_i - v_i),$$
$$L_i = P_{ij}\hat{n}_j + \rho u_i(u_n - v_n). \tag{7}$$

The square brackets in (6) denote that the kernels of integrals are computed at the corresponding retarded time which is defined as follows:

$$\tau = t - \frac{r}{a_0}. \tag{8}$$

The various subscripted quantities appearing in (6) are the inner products of a vector and a unit vector implied by the subscript. For example,

$$L_r = \vec{L}\cdot\vec{r} = L_i r_i, \qquad U_n = \vec{U}\cdot\vec{n} = U_i n_i, \tag{9}$$

where $\vec{r}$ and $\vec{n}$ denote the unit vectors in the radiation and the wall normal directions, respectively. The dot over a variable denotes source-time differentiation of that variable.

Using the URANS calculations after the fluctuating variables stability, pressure and velocity fluctuations upon the impeller surfaces have been extracted for 2000 time steps. Then, sound pressure signals are computed at the receiver location using the source data collected during the aerodynamic calculations. It is important to state that the presence of the volute casing is neglected in this approach (free-field radiation). For this reason, the acoustic pressure calculations have been carried out at the position shown in Figure 7.

6. AERODYNAMIC RESULTS AND DISCUSSION

The aerodynamic characteristics of the studied fans are given in Table 2. It can be seen that the VA160D fan (with irregular blade spacing) has the same characteristics as the reference fan (VA160). This result indicates that alterations in blade spacing do not significantly alter the aerodynamic characteristics of the fan.

Compared to the other fans, the VA150 presents better efficiency because of its smaller outlet radius which contributes to minimizing the shaft torque applied on the rotating blades. However, the pressure decrease is compensated

Table 2: Aerodynamic characteristics.

Fan	N (rpm)	ΔP_s (num.)	ΔP_s (exp.)	η (%)
VA160	3000	682	681	51
VA160D	3000	679	680	51
VA150	3200	700	684	54
VA160E	2900	640	678	52

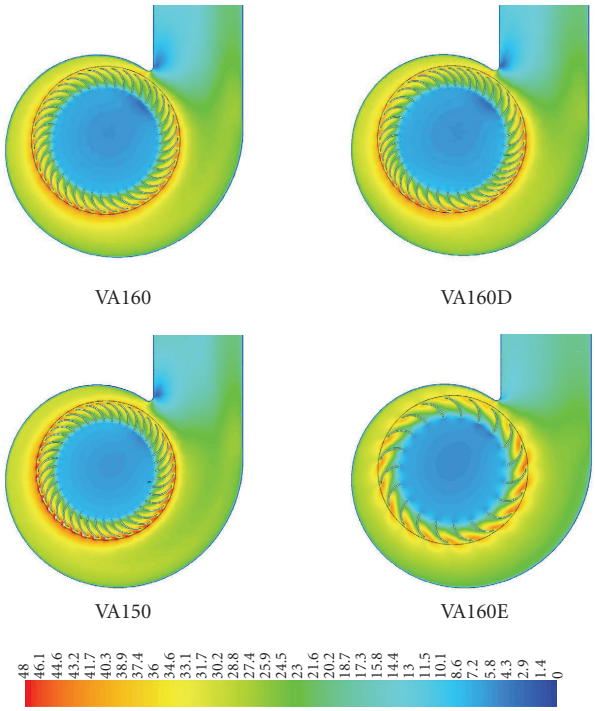

Figure 8: Instantaneous velocity field at the meridian surface (0.14 seconds).

by increasing the rotational speed to 3200 rpm. In addition to this, the VA160E fan presents a better efficiency compared to the VA160 and VA160D fans. Indeed, reducing the number of blades contributes to minimizing aerodynamic losses through the impeller blades grid. Then, to generate the requested fan characteristic (680 Pa), the impeller rotational speed is decreased to 2900 rpm.

Figure 8 shows the instantaneous velocity field at the median surfaces of the VA160, VA160D, VA150, and VA160E fans, respectively. According to these figures, the conversion of dynamic pressure produced by the impeller rotation into static pressure by the volute casing can be seen. A nonhomogeneous velocity distribution is observed at the zone around the gap between volute tongue and impeller periphery, characterized by a high gradient of velocity. The volute tongue whose role is to drive the flow towards the fan outlet also presents a singularity for the flow. The shape of the volute casing creates a geometrical asymmetry which influences the velocity and pressure distributions.

The comparison between the VA160 and VA160D fans shows that alterations in blade spacing do not significantly alter the overall flow field of the fan. On the other hand, the VA150 fan presents a more homogeneous flow field around the impeller periphery and particularly at the volute tongue zone. In this configuration, the interactions between the volute tongue and the rotating blades are minimized by reducing the radial distance between the volute tongue and the impeller periphery.

According to Figure 8, the VA160E with the smaller number of blades generates a nonhomogeneous flow field particularly at the impeller periphery. A similar result has been shown in [14] concerning the influence of the blades number on the flow field of a centrifugal pump.

7. WALL PRESSURE FLUCTUATIONS AND SPECTRAL ANALYSIS

The time histories of the pressure fluctuation at the investigated nodal points on the volute tongue are shown in Figure 9 with their corresponding spectral analysis. The numerical results are compared to the experimental data. Concerning the VA160 and VA150 fans, a good agreement has been found between the measured data and the numerical calculations particularly at the blade-passing frequency (BPF) and at lower frequencies. The spectra of the pressure fluctuation level computed and measured on these fans suggest that the dominant mode occurs at 1950 Hz and 2080 Hz, respectively. These frequencies correspond to the BPF point. The absence of other dominant peaks in the spectra at the harmonic frequencies is observed. This is due to the nature of the interaction between the impeller and the volute tongue which generates small interferences. Thus, the corresponding harmonics are hidden by the broadband signal components. The main interactions which could produce tonal component in the signal are due to the presence of the volute tongue near the impeller periphery. The pressure fluctuation level at the BPF spectrum is higher for VA160 than VA150. The VA150 presents smaller radial distance between the impeller and the volute tongue, and the aerodynamic interactions between the rotating and stationary zones are less important.

Concerning the VA160D fan behavior, the wall pressure fluctuations are underestimated by the measurements. For these high-pressure fluctuations, the pressure microphone is saturated, and the real signal is not read adequately. This phenomenon is illustrated by the comparison between the numerical and the experimental signals amplitude versus time. However, the overall form of the experimental signal is in good agreement with the CFD predictions. The temporal signals clearly show a passage of all the three blade blocs per revolution which correspond to the three lobe patterns with 150 Hz. On the other hand, the split discrete frequencies are separated by multiples of 150 Hz from the BPF.

Concerning the unsteady pressure generated by the VA160E fan, the phenomenon due to the microphone saturation is observed. Two high dominant peaks are observed at the BPF (950 Hz) and at the second harmonic frequency (1900 Hz). It can be seen that the pressure fluctuation level at these frequencies is higher for VA160E than for VA150.

Finally, the analysis of the four spectra shows that the numerical and experimental data do not match beyond a

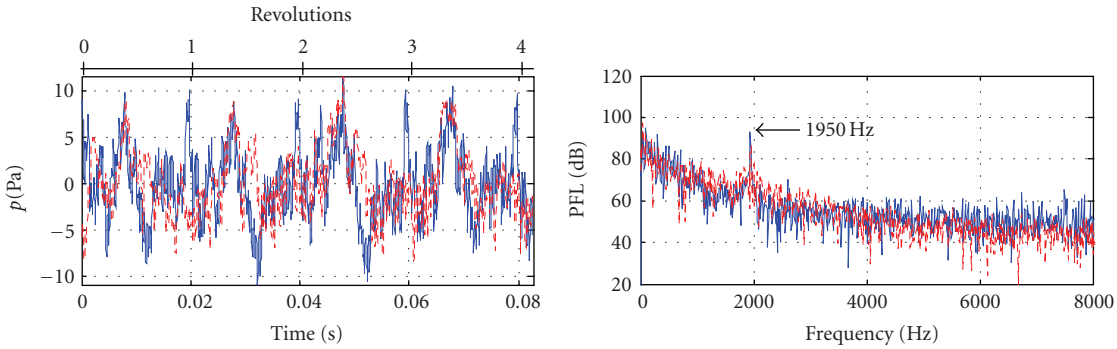

(a) VA160

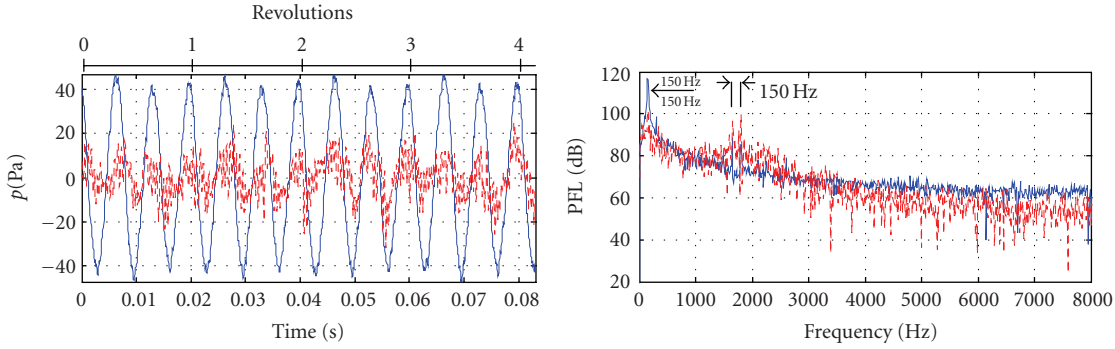

(b) VA160D

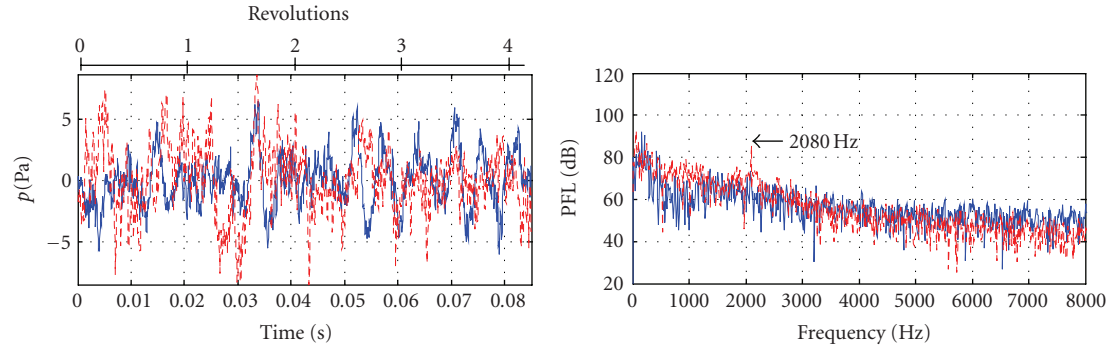

(c) VA150

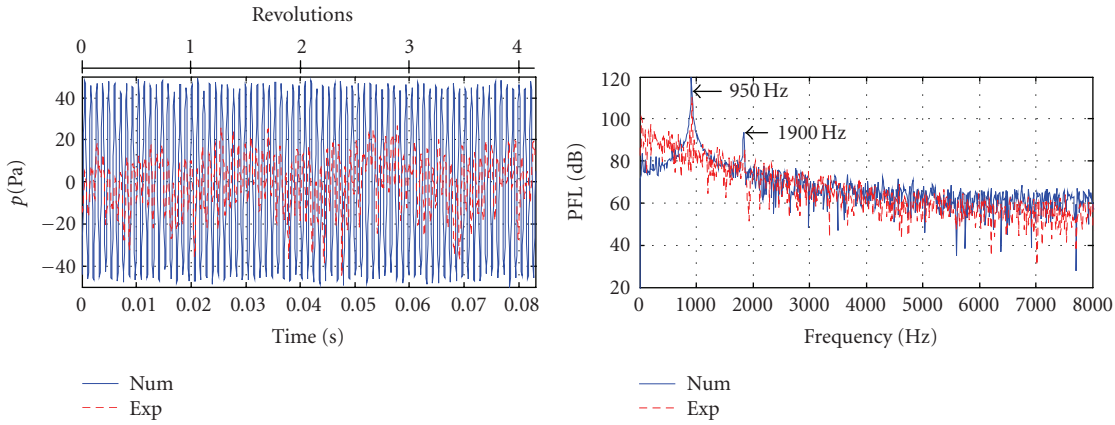

(d) VA160E

Figure 9: Wall pressure fluctuations with corresponding spectral analysis (VA160, VA160D, VA150, and VA160E) (frequency resolution = 12.5 Hz).

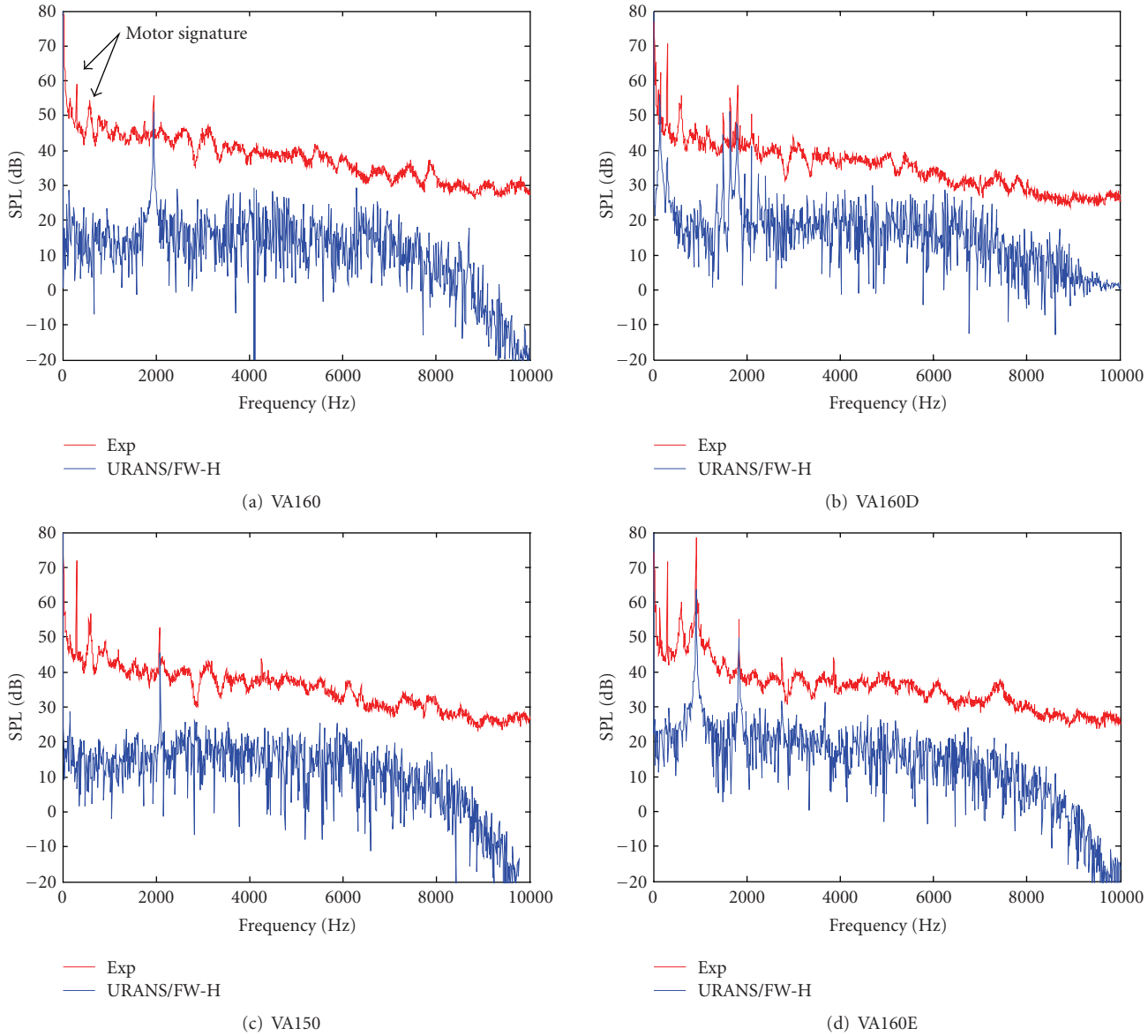

Figure 10: Acoustic pressure of the investigated fans—(frequency resolution = 12.5 Hz).

certain frequency (around 4000 Hz). This cutoff frequency is related to the mesh resolution, and it represents the upper limit of frequency resolvable by the used numerical modeling. Finer mesh grid coupled with large Eddy simulation (LES) calculations could improve the matching between these results. Thus, the numerical results obtained in the frequency range from 4000 Hz to 8000 Hz have no physical significance. This part of the signal which is called "numerical noise" is due to the numerical processing effects. Therefore, the maximum frequency F_{MC} reasonably resolved by the local grid spacing Δ is [15]

$$F_{MC} = \frac{u'}{2\Delta}. \quad (10)$$

On the other hand, the forward curved blades suffer from severe complex phenomena related to the flow separation and also to the inlet blade angle which leads to strong interactions between fluid particles and blades leading edge. These phenomena cannot be modeled adequately by the URANS approach.

8. ACOUSTIC RESULTS AND DISCUSSION

The acoustic signals generated by the four investigated fans are shown in Figures 10(a), 10(b), 10(c), and 10(d), respectively. The experimental data are compared to the URANS/FW-H calculations. The analysis of these signals obtained at far field shows a correlation between the unsteady pressures acquired at the near field and at the far field. Thus, the remarks cited in the wall pressure fluctuation level section are valid also in the present section. The four signals show two peaks at 300 Hz and 600 Hz, respectively, related

Table 3: Numerical and experimental SPL values (VA160).

		SPL (dB)	
VA160	Frequencies	EXP.	URANS/FW-H
	1950 Hz	57	51

Table 4: Numerical and experimental SPL values (VA160D).

		SPL (dB)	
VA160D	Frequencies	EXP.	URANS/FW-H
	1500 Hz	51	44
	1650 Hz	55	52
	1800 Hz	57	47

Table 5: Numerical and experimental SPL values (VA150).

		SPL (dB)	
VA150	Frequencies	EXP.	URANS/FW-H
	2080 Hz	53	45

Table 6: Numerical and experimental SPL values (VA160E).

		SPL (dB)	
VA160E	Frequencies	EXP.	URANS/FW-H
	950 Hz	78	64
	1900 Hz	55	50

to the fan motor signature which does not depend on the rotational speed.

Tables 3, 4, 5, and 6 show the comparison between the numerical and experimental results at the remarkable frequencies. (BPF and its harmonics) of the investigated fans. It can be seen that the SPL values given by the numerical calculations are lower than the measured data (~5 to 8 dB). These differences partially represent the reflections and reverberations of the experimental facility which are not taken into account in the FW-H equation (free field radiation). On the other hand, the numerical modeling has not been used in order to predict the broadband noise. According to [13], URANS calculations cannot adequately provide the surface pressure fluctuations needed for broadband noise prediction. This remark explains the differences on the broadband signals components found between the numerical and the experimental results. Thus, the significant part of the predicted acoustic signals consists of the tonal noise generated by the flow unsteadiness and the interactions between rotating blades and volute casing.

According to Table 4, the VA150 fan generates lower SPL than VA160 fan showing that reduction of the distance between the blade periphery and the volute tongue allows minimizing the generated tonal noise (~4 dB at the BPF).

Concerning the VA160E fan, it gives the highest SPL compared to the other fans. This result shows that the reduction of the number of blades generates strong aerodynamic interactions (between volute tongue and rotating blades) which contribute to accentuating the tonal noise at the BPF.

9. CONCLUSION

The influence of design parameters on the unsteady flow in a centrifugal fan has been studied in this paper using numerical and experimental investigations. The study showed the effects related to irregular blade spacing, blades number, and radial distance between the impeller periphery and the volute tongue. A correlation between the wall pressure fluctuations and the far field noise signals has been found.

It should be interesting to extend this work by the following:

(i) using large Eddy simulation (LES) approach to feed acoustic models;

(ii) using laser Doppler velocimetry (LDV) and particle image velocimetry (PIV) techniques in order to investigate the unsteady velocity field;

(iii) including the casing effect in the FW-H equation.

NOMENCLATURE

a_0: Far field sound speed [m/s]
$f = 0$: Function that describes the source surface: impeller blades surfaces [−]
F: Frequency [Hz]
F_{MC}: Mesh cutoff frequency [Hz]
G: Green's function = $\tau - t + r/c$ [−]
$H(f)$: Heaviside function [−]
k: Blades distribution coefficient [−]
M: Local Mach number vector of source with respect to a frame fixed to the undisturbed medium, with components M_i [−]
N: Rotational speed [rpm]
n: Blades repetition number [−]
n_j: Unit normal vector [−]
p': Acoustic pressure [Pa]
P_{ij}: Compressive stress tensor [Pa]
p_{ref}: Reference pressure [Pa]
r: Distance between observer and source [m]
R_2: Impeller outlet radius [m]
t: Observer time [s]
T_{ij}: Lightill stress tensor [Pa]
u': velocity perturbation [m/s]
u_i: Fluid velocity in the x_i direction [m/s]
u_n: Fluid velocity in the normal direction [m/s]
v_i: Surface velocity in the x_i direction [m/s]
v_n: Surface velocity in the normal direction [m/s]
x: Observer position vector [m]
z: Blades count
$\delta(f)$: Dirac delta function [−]
Δ: cell dimension [mm]
ΔP_s: Static pressure generated by the fan [Pa]
ΔS: Cell grid size at the impeller periphery [mm]
Δt: Time step [s]
$\Delta\theta_b$: Blade spacing angle [degree]
ρ: Density [kg/m^3]
τ: Source time [s]
η: Efficiency [%].

SUBSCRIPTS

b: Blade count
L: Loading noise component
T: Thickness noise component
0: Denotes fluid variable in quiescent medium.

ACKNOWLEDGMENT

The authors wish to thank the (Institut de Recherche et Coordination Acoustique/Musique) (IRCAM) for allowing them to use its anechoic room.

REFERENCES

[1] ISO 5801, "Industrial fans—performance testing using standardized airways," 1997.
[2] M. Boltezar, M. Mesaric, and A. Kuhelj, "The influence of uneven blade spacing on the SPL and noise spectra radiated from radial fans," *Journal of Sound and Vibration*, vol. 216, no. 4, pp. 697–711, 1998.
[3] W.-H. Jeon, "A numerical study on the effects of design parameters on the performance and noise of a centrifugal fan," *Journal of Sound and Vibration*, vol. 265, no. 1, pp. 221–230, 2003.
[4] M. V. Lowson, "The sound field for singularities in motion," *Proceedings of the Royal Society in London, Series A*, vol. 286, no. 1407, pp. 559–572, 1965.
[5] Y. Cho and Y. J. Moon, "Discrete noise prediction of variable pitch cross-flow fans by unsteady Navier-Stokes computations," *Journal of Fluids Engineering*, vol. 125, no. 3, pp. 543–550, 2003.
[6] R. Ballesteros-Tajadura, S. Velarde-Suárez, J. P. Hurtado-Cruz, and C. Santolaria-Morros, "Numerical calculation of pressure fluctuations in the volute of a centrifugal fan," *Journal of Fluids Engineering*, vol. 128, no. 2, pp. 359–369, 2006.
[7] M. Younsi, F. Bakir, S. Kouidri, and R. Rey, "2D and 3D unsteady flow in squirrel-cage centrifugal fan and aeroacoustic behavior," in *Proceedings of the 2nd Joint U.S.-European Fluids Engineering Division Summer Meeting (FEDSM '06)*, pp. 805–813, Miami, Fla, USA, July 2006.
[8] M. Younsi, F. Bakir, S. Kouidri, and R. Rey, "Numerical and experimental study of unsteady flow in centrifugal fan," in *Proceedings of the 7th European Turbomachinery Conference (ETC '07)*, Athens, Greece, March 2007.
[9] K. Majidi, "Numerical study of unsteady flow in a centrifugal pump," *Journal of Turbomachinery*, vol. 127, no. 2, pp. 363–371, 2005.
[10] F. R. Menter, "Zonal two equations k-ω turbulence models for aerodynamic flows," in *Proceedings of the 24th AIAA Fluid Dynamics Conference*, Orlando, Fla, USA, July 1993, AIAA paper 93-2906.
[11] J. E. Bardina, T. J. Huang, and T. J. Coakley, "Turbulence modeling, validation, testing and development," NASA Technical Memorandum 110446, NASA, Washington, DC, USA, 1997.
[12] J. E. Ffowcs Williams and D. L. Hawkings, "Sound generation by turbulence and surfaces in arbitrary motion," *Philosophical Transactions of the Royal Society of London. Series A*, vol. 264, no. 1151, pp. 321–342, 1969.
[13] K. S. Brentner and F. Farassat, "Analytical comparison of the acoustic analogy and Kirchhoff formulation for moving surfaces," *AIAA Journal*, vol. 36, no. 8, pp. 1379–1386, 1998.
[14] G. Kergourlay, M. Younsi, F. Bakir, and R. Rey, "Influence of splitter blades on the flow field of a centrifugal pump: test-analysis comparison," *International Journal of Rotating Machinery*, vol. 2007, Article ID 85024, 13 pages, 2007.
[15] F. Mendonça, A. Read, S. Caro, K. Debatin, and B. Caruelle, "Aeroacoustic simulation of double diaphragm orifices in an aircraft climate control system," in *Proceedings of the 11th AIAA/CEAS Aeroacoustics Conference*, Monterey, Calif, USA, May 2005, AIAA paper 2005-2976.